

Screened Thin-Target Bremsstrahlung with Partially-Ionized High-Z Species

S. Guinchard,¹ Y. Savoye-Peysson,² and J. Decker¹

¹*Ecole Polytechnique Fédérale de Lausanne (EPFL),
Swiss Plasma Center (SPC), CH-1015, Lausanne, Switzerland*

²*CEA, IRFM, F-13108, Saint-Paul-lez-Durance, France*

Bremsstrahlung emission remains a cornerstone process in the characterization of electron dynamics in diverse high-energy environments. In particular, the accurate description of thin-target electron-ion bremsstrahlung in the presence of high- Z species requires careful treatment of atomic screening effects, especially when atoms are partially ionized. We present a fully analytic screening model based on a multi-Yukawa representation of the atomic potential, enabling the calculation of bremsstrahlung cross sections for arbitrary nuclear charge and ionization state, and electron energies up to a few tens of MeV. This framework extends prior treatments of neutral atoms to include partially ionized high- Z elements in a fully analytic framework.

Keywords: Bremsstrahlung, Born approximation, Cross section, QED, Relativistic scattering, Screened bremsstrahlung, Furry–Sommerfeld–Maue.

I. INTRODUCTION

Accurate and computationally efficient descriptions of thin-target bremsstrahlung remain a central objective of theoretical and applied radiation physics. Building on the foundational analyses of Sauter [Sau34], Bethe–Heitler [BH34], and Racah [Rac34], together with practical prescriptions such as the so-called additivity rule [OMW57] and atomic models for screening [Tho27, Fer28, Mol47], modern studies concentrate on two tightly interwoven challenges: (i) the systematic inclusion of Coulomb distortion beyond the first Born approximation in a form that remains analytically tractable, and (ii) a faithful representation of atomic screening that smoothly covers charge states from neutral atoms to highly stripped ions. Both challenges are essential for constructing a single method that can reproduce experiments and benchmark calculations across the largest possible range of parameters.

The theoretical basis for such developments is the scattering-theory framework in which bremsstrahlung cross sections follow from Fermi’s golden rule [Fer50, Sch68] (see Sec. II). In this paper we restrict attention to the thin-target, single-collision regime for electron energies up to a few tens of MeV, where quantum-coherence suppression effects (e.g. Landau–Pomeranchuk–Migdal [LP53b, LP53a, Mig56]) are negligible. We note that fully rigorous S-matrix (Furry-picture) treatments [Fur51, JR55], coupled to double Dirac partial-wave (PW) expansions (the route pioneered by Tseng & Pratt [TP71], and developed by Pratt and collaborators [LKPT76, PTL+77]) provide the most accurate nuclear-bremsstrahlung results available, but they require heavy numerical machinery and become prohibitive as the number of required PW increases exponentially with energy [PT75, YS10, JA21]. We do not consider that PW S-matrix route in the present work. In-

stead, we focus on analytic and semi-analytic expressions that are directly compatible with our screening ansatz.

A recurring limitation of analytic bremsstrahlung treatments is the incorporation of screening. Classical prescriptions (Molière parameterizations [Mol47], Thomas–Fermi–like screening lengths [Tho27, Fer28], and tabulated atomic form factors [HVB+75, SMMP87]) describe neutral-atom behavior but do not by themselves provide a compact analytic route to interpolate across charge states. Alternative analytic screening laws have also been proposed, such as the Thomas–Fermi–Kirillov form (TFK), which replaces the Yukawa exponential by a power $n = 3/2$ [KTT75], see Eq. (11), but these remain difficult to integrate consistently into bremsstrahlung cross section formalisms. Model-potential approaches, most notably that of Avdonina and Pratt [AP93], provide analytic screened atomic form factors (AFF) and explicitly address ionic charge states, demonstrating that screening significantly alters spectral and polarization observables. Their framework, however, relies on a specific one-parameter potential and is not easily generalized to reproduce high-quality tabulations or to interpolate smoothly between neutral and bare-ion limits. At the same time, investigations of Coulomb corrections emphasize that screening and higher-order distortion must be treated together to achieve percent-level accuracy in the application-relevant ~ 1 –100 MeV window and for moderate to high- Z targets [RDP72, MM16].

To overcome these difficulties, we introduce an analytic AFF representation built from a finite sum of Yukawa screening potentials [Hau08, SPMB+23]. Each term admits a simple analytic momentum-space component suitable for insertion into differential cross sections, while the linear combination can be fitted to high-quality atomic data (Dirac–Hartree–Fock–Slater (DHFS) fits [SMMP87, FTS+16, FGJB19] or Hubbell tabulations [HVB+75]) and adjusted to account for removed bound charge, thereby extending from neutral atoms to fully stripped ions. Practically, screening is implemented by inserting the fitted multi-Yukawa (MY) form factor into the Bethe–Heitler (BH) differential cross section while higher-order Coulomb distortion is re-

tained through the Roche–Ducos–Prorior (RDP) expression for the unscreened contribution [RDP72]. Following the Olsen–Maximon–Wergeland (OMW) additivity rule [OMW57] (see Sec. II), the screened doubly differential cross section is obtained as the sum of the unscreened expression in a pure Coulomb field, and a screening correction in the first Born approximation, such that both neutral-atom and bare-nucleus limits are preserved. The result is a compact, rapidly evaluable expression for the doubly differential cross section (DDCS) that is inexpensive compared with full PW models.

The motivation for such a compact and accurate treatment spans several application domains. Relativistic electrons physics in nuclear fusion experiments [PD08], radiation-safety calculations, and astrophysical radiative-transfer problems [KMTY88, CRB20], among others, all require reliable bremsstrahlung cross sections for partially ionized targets. Recent advances in unified atomic physics models for Fokker–Planck solvers [SPMB+23], underline the need for analytic parameterizations that interpolate smoothly across charge states without reliance on large precomputed databases such as open-ADAS [Sum04]. The present scheme is designed for direct integration into such kinetic and transport frameworks, offering fast evaluation and high accuracy.

The aims of the paper are therefore: (i) to present the multi-Yukawa AFF representation as a practical model for screening across ionization degrees; (ii) to derive bremsstrahlung differential cross sections obtained by combining this representation with a Sommerfeld–Maue-based formalism and consistent Coulomb corrections following the OMW additivity rule; and (iii) to validate the resulting scheme through systematic comparisons with existing models and experiments [Mot55, SK56, RD67, RE72, PT75]. The rest of the paper is organized as follows. Section II recalls the unscreened bremsstrahlung formalism from Fermi’s golden rule, and introduces the unscreened components of the model, namely the RDP and unscreened BH differential cross sections. Section III defines the MY AFF and incorporates it in the derivation of the DDCS. Section IV presents the numerical results and comparisons with experiments, and Section V summarizes conclusions and outlines future applications.

II. THEORETICAL FRAMEWORK FOR ELECTRON–ION BREMSSTRAHLUNG

In the present work, we assume that the reader is familiar with the theory of bremsstrahlung, and in

particular with how the differential cross sections for bremsstrahlung interactions are derived. We recall that all formulae considered in this work originate from Fermi’s *golden rule* [Fer50, Sch68] that we remind here:

$$\frac{d^3\sigma_{e-i}}{dkd\Omega_kd\Omega_p} := \frac{\alpha}{(2\pi)^4}\lambda_C^2\frac{E_0Epk}{p_0}\frac{1}{2}\sum_{s,s_0,\mathbf{e}^*}|M|^2 \quad (1)$$

$$M := \int \psi^\dagger(\mathbf{r})(\boldsymbol{\alpha}\cdot\mathbf{e}^*)e^{-i\mathbf{k}\cdot\mathbf{r}}\psi_0(\mathbf{r})d^3\mathbf{r}.$$

The symbols involved are the usual for the context: σ_{e-i} denotes the cross section, α is the fine structure constant and $\lambda_C = \hbar/m_e c^2$ the reduced Compton wavelength of the electron. Ω_k, Ω_p denote the solid angles of emission for the photon and scattering of the electron, respectively, while k is the radiated photon energy. The electron final and initial energies are E, E_0 , respectively, and the same applies for the momenta p, p_0 and wave functions ψ, ψ_0 . The squared matrix elements amplitudes $|M|^2$ are summed over the final and initial electron spin states s, s_0 , as well as polarization vector of the photon \mathbf{e}^* . The reason for this averaging is that none of these quantities are observed. Finally, $\boldsymbol{\alpha}$ denotes the Dirac matrices. Note that throughout the work, energies and momenta are expressed in relativistic units, normalized to $m_e c^2$ and $m_e c$, respectively. Coordinates are expressed in units of the reduced Compton wavelength λ_C such that wave factors take the form $\exp(i\mathbf{k}\cdot\mathbf{r})$.

The triply-differential cross section (TDCS) in Eq. (1) involves an integral over all space of the initial and final electron wave functions. In the vicinity of the nucleus, the nuclear (Coulomb) effects are important, while further from it, the electrons bound to the nucleus may screen the potential of the latter, so that a screening correction to the pure Coulomb field cross section ought to be considered. Olsen, Maximon and Wergeland noted that for the DDCS, i.e. after integrating out the electron’s degrees of freedom, and for energies greater than the electron rest mass, the screening correction to the Coulomb cross section is additive [OMW57]:

$$\left(\frac{d^2\sigma_{e-i}^{Z_s}}{dkd\Omega_k}\right)^s \simeq \left(\frac{d^2\sigma_{e-i}^Z}{dkd\Omega_k}\right)_{\text{Coul}}^{\text{us}} + \left[\left(\frac{d^2\sigma_{e-i}^{Z_s}}{dkd\Omega_k}\right)_{\text{Born}}^s - \left(\frac{d^2\sigma_{e-i}^Z}{dkd\Omega_k}\right)_{\text{Born}}^{\text{us}}\right]. \quad (2)$$

The latter is the so-called OMW *additivity rule*. The

term in brackets is the screening correction. The su-

perscripts ‘‘s’’ and ‘‘us’’ mean screened and unscreened, respectively. An illustrating figure is presented at the beginning of Section IV, while a discussion on the validity of the OMW rule can be found in [JAM19]. We now introduce the expressions we will consider for the terms from Eq. (2).

A. Bethe–Heitler Cross Section

As discussed in the introduction to this paper, the triply differential cross section (differential in the photon energy, the photon emission solid angle, and the electron scattering solid angle) as derived by Bethe and Heitler [BH34] and labeled 1BS in Ref. [KM59], provides the general expression for bremsstrahlung in the first Born approximation. It is given by

$$\left(\frac{d^3 \sigma_{e-i}^{Z_s}}{dk d\Omega_k d\Omega_p} \right)_{\text{BH}} = \alpha \left(\frac{r_e}{2\pi} \right)^2 Z_s^2 (1 - F_{Z_s}(q))^2 \times \frac{p}{k p_0 q^4} A^{\text{BH}}, \quad (3)$$

with r_e the classical electron radius, and where F_{Z_s} is the atomic form factor (AFF). The latter is set to zero in the unscreened case, and we retain this expression for the unscreened bremsstrahlung term, i.e. the third on the right-hand side of Eq. (2). The recoil momentum transferred to the nucleus, q , is given by the relation

$$\mathbf{q} = \mathbf{p} - \mathbf{p}_0 - \mathbf{k},$$

such that

$$q^2 = p_0^2 + p^2 + k^2 - 2p_0 k \cos \theta_0 + 2pk \cos \theta - 2pp_0 (\cos \theta \cos \theta_0 + \sin \theta \sin \theta_0 \cos \phi),$$

where θ_0 and θ denote the angles between the emitted photon and the incoming and scattered electron momenta, respectively, and ϕ is the angle between the planes $(\mathbf{p}_0, \mathbf{k})$ and (\mathbf{p}, \mathbf{k}) . Here, and from now on, $Z_s := Z - N_s$ represents the effective ionic charge of the species, that is, the atomic number minus the number of bound electrons. The term A^{BH} in Eq. (3) is given by

$$A^{\text{BH}} = \sum_{n=1}^4 A_n^{\text{BH}},$$

where

$$A_1^{\text{BH}} = \frac{p^2 \sin^2 \theta}{(E - p \cos \theta)^2} (4E_0^2 - q^2) \quad (4a)$$

$$A_2^{\text{BH}} = \frac{p_0^2 \sin^2 \theta_0}{(E_0 - p_0 \cos \theta_0)^2} (4E^2 - q^2) \quad (4b)$$

$$A_3^{\text{BH}} = 2k^2 \frac{p^2 \sin^2 \theta + p_0^2 \sin^2 \theta_0}{(E - p \cos \theta)(E_0 - p_0 \cos \theta_0)} \quad (4c)$$

$$A_4^{\text{BH}} = - \frac{2pp_0 \sin \theta \sin \theta_0 \cos \phi}{(E - p \cos \theta)(E_0 - p_0 \cos \theta_0)} (2E^2 + 2E_0^2 - q^2). \quad (4d)$$

For certain combinations of energies, momenta and angles, the expressions (4a)–(4d) exhibit near exact cancellations, and careful numerical treatment is required when evaluating the expression as is. This issue has been discussed in detail by Maximon *et al.* [MdAG87], who proposed a refactored formulation to overcome this caveat. In the present work, this difficulty does not arise in that the integrations performed for both the unscreened and screened cases do not exhibit such canceling terms.

In the unscreened limit ($F_{Z_s} = 0$), Eq. (3) can be integrated analytically over all the possible scattering directions, recalling that $d\Omega_p = \sin \theta d\theta d\phi$. The integration has first been done by Sauter [Sau34], and the result is denoted 2BN in Ref. [KM59]. We will refer to the DDCS without screening as the Sauter (S) formula, even though it comes from integration of the Bethe–Heitler TDCS. It reads

$$\left(\frac{d^2 \sigma_{e-i}^Z}{dk d\Omega_k} \right)_S^{\text{us}} = \int \left(\frac{d^3 \sigma_{e-i}^Z}{dk d\Omega_k d\Omega_p} \right)_{\text{BH}} d\Omega_p = \alpha r_e^2 \frac{Z^2}{8\pi} \frac{p}{k p_0} \sum_{n=1}^{10} B_n^{\text{S}}, \quad (5)$$

where

$$B_1^{\text{S}} = \frac{8 \sin^2 \theta_0}{p_0^2 \Delta_0^4} (2E_0^2 + 1)$$

$$B_2^{\text{S}} = - \frac{2(5E_0^2 + 2EE_0 + 3)}{p_0^2 \Delta_0^2}$$

$$B_3^{\text{S}} = - \frac{2(p_0^2 - k^2)}{Q^2 \Delta_0^2}$$

$$B_4^{\text{S}} = \frac{4E}{p_0^2 \Delta_0}$$

$$B_5^{\text{S}} = \frac{L}{pp_0} \frac{4E_0 \sin^2 \theta_0 (3k - p_0^2 E)}{p_0^2 \Delta_0^4}$$

$$B_6^{\text{S}} = \frac{L}{pp_0} \frac{4E_0^2 (E_0^2 + E^2)}{p_0^2 \Delta_0^2}$$

$$B_7^{\text{S}} = \frac{L}{pp_0} \frac{2 - 2(7E_0^2 - 3EE_0 + E^2)}{p_0^2 \Delta_0^2}$$

$$B_8^{\text{S}} = \frac{L}{pp_0} \frac{2k(E_0^2 + EE_0 - 1)}{p_0^2 \Delta_0}$$

$$B_9^{\text{S}} = - \frac{4\epsilon}{p \Delta_0}$$

$$B_{10}^{\text{S}} = \frac{\epsilon^Q}{pQ} \left[\frac{4}{\Delta_0^2} - \frac{6k}{\Delta_0} - \frac{2k(p_0^2 - k^2)}{Q^2 \Delta_0} \right],$$

with

$$L = \ln \left(\frac{EE_0 - 1 + pp_0}{EE_0 - 1 - pp_0} \right),$$

$\Delta_0 = E_0 - p_0 \cos \theta_0$, and $Q^2 = p_0^2 + k^2 - 2p_0 k \cos \theta_0$. In addition,

$$\epsilon = \ln \left(\frac{E+p}{E-p} \right) \quad \text{and} \quad \epsilon^Q = \ln \left(\frac{Q+p}{Q-p} \right).$$

The first Born approximation, and thus the Bethe–Heitler–Sauter cross section of Eq. (5), is valid only when $\alpha Z \ll (\beta_0, \beta)$, a very restrictive condition. Under this approximation, the Born formulas yield cross sections larger than experimental values in the soft-photon limit ($k \ll E$), but fall below them in the tip (high frequency) region, where the predicted cross section goes to zero as the photon energy reaches the incident energy.

B. Sauter–Elwert Cross Section

As discussed previously, in the short-wavelength limit ($k \uparrow E$), the Born-approximation doubly differential cross section (DDCS) fails, vanishing as the photon energy approaches the incident electron energy. However, the cross section remains finite if it is multiplied by an appropriate Coulomb correction factor derived by Elwert and Haug [EH69],

$$F_E(p_0, p, Z) = \frac{\xi}{\xi_0} \frac{1 - \exp(-2\pi\xi_0)}{1 - \exp(-2\pi\xi)},$$

where $\xi_0 = \alpha Z E_0 / p_0 = \alpha Z \beta_0^{-1}$ and $\xi = \alpha Z \beta^{-1}$. The resulting Sauter–Elwert (SE) cross section is then defined as

$$\left(\frac{d^2 \sigma_{e-i}^Z}{dk d\Omega_k} \right)_{SE}^{us} := F_E(p_0, p, Z) \left(\frac{d^2 \sigma_{e-i}^Z}{dk d\Omega_k} \right)_S^{us}. \quad (6)$$

Physically, the Elwert factor F_E accounts for the Coulomb distortion of the initial and final electron wave functions. It acts at the triply differential level where it modifies the local transition probability density. When F_E is applied to the TDCS and one integrates over the outgoing electron angle Ω_p to obtain the DDCS, the resulting expression becomes essentially independent of the photon direction Ω_k in the neighborhood of the long-wavelength limit. As ξ_0 decreases, this angular independence extends progressively toward the short-wavelength limit [Elw39]. This near-constancy allows F_E to be treated as a global multiplicative factor that can be pulled out of the angular integration, yielding the compact form in Eq. (6). At shorter wavelengths, however, where the outgoing electron becomes slow and Coulomb distortion is strongest, this approximation breaks down and F_E must in principle be retained inside the angular integrals. Elwert and Haug [EH69] addressed this by computing numerical Coulomb factors that extend the validity of the correction into the short-wavelength regime.

The Sauter–Elwert cross section is valid in the non-relativistic regime ($\xi_0 \ll 1$) and for sufficiently small atomic numbers ($Z \lesssim 26$). Unlike the Sauter result, it does not vanish at the tip region. For a more detailed discussion on Coulomb factors, we refer to [Elw39, EH69].

For highly relativistic incident electrons, and higher atomic numbers, the Sauter–Elwert corrected cross section becomes inadequate and more advanced numerical

treatments of the Coulomb field, such as the Roche–Ducos–Proriol cross section, are required.

C. Roche–Ducos–Proriol Cross Section

For high- Z species ($Z > 26$), the Sauter expression corrected within the first Born approximation (with Elwert factors) is no longer reliable, particularly in the tip region (see Sec. II B). In such cases one must turn to formulations that treat the Coulomb field more precisely. The first analytic progress in this direction was made by Elwert and Haug, who derived their cross section using Furry–Sommerfeld–Maue (FSM) (usually simply called Sommerfeld–Maue (SM)) wave functions [Fur34, SM35] for the electron in the pure Coulomb potential [EH69]. This approach was later taken to the next order by Roche, Ducos, and Proriol, who added the dominant higher-order terms beyond Elwert–Haug [RDP72]. Despite its extensive use in the literature [Hau08, MM16, MM17, MJA17], the RDP cross section as introduced in the original source [RDP72] is not consistent, as its mixed-order character (combining third- and fourth-order contributions) does not necessarily lead to improved accuracy, as originally claimed. Although the mixed-order aspect of the initial formalism had been justified previously [Hau08, MM16, MM17, MJA17], the resulting inconsistency was later identified and corrected at the level of the radiation matrix element by Jakubassa-Amundsen and Mangiarotti [JAM19]. Here, we extend this correction to the level of the triply-differential cross section, yielding a consistently truncated third-order expression. The corrected RDP formalism provides the most accurate closed-form description of bremsstrahlung in a pure Coulomb field in the energy range from a few to several tens of MeV, and the integrated RDP TDCS is the expression we employ for the first term on the right-hand side of Eq. (2). The RDP cross section reads

$$\left(\frac{d^3 \sigma_{e-i}^Z}{dk d\Omega_k d\Omega_p} \right)_{RDP}^{us} := \frac{d^3 \sigma_{RDP,1}^Z}{dk d\Omega_k d\Omega_p} + \frac{d^3 \sigma_{RDP,2}^Z}{dk d\Omega_k d\Omega_p}. \quad (7)$$

The first term on the right-hand side is identical to the cross section derived by Elwert and Haug [EH69],

$$\frac{d^3 \sigma_{RDP,1}^Z}{dk d\Omega_k d\Omega_p} \equiv \frac{d^3 \sigma_{EH}^Z}{dk d\Omega_k d\Omega_p},$$

while the second term, using the Bethe–Maximon method [BM54], describes higher-order corrections. From Refs.

[RDP72, Hau08],

$$\begin{aligned}
\frac{d^3\sigma_{\text{RDP},1}^Z}{dkd\Omega_k d\Omega_p} &= \frac{\alpha Z^2}{\pi^2} r_e^2 \frac{kp}{p_0} N \{ [E_0 E - 1 \\
&\quad - (\hat{\mathbf{k}} \cdot \mathbf{p}_0) (\hat{\mathbf{k}} \cdot \mathbf{p})] |J_1|^2 \\
&\quad + [E_0 E + 1 + (\hat{\mathbf{k}} \cdot \mathbf{p}_0) (\hat{\mathbf{k}} \cdot \mathbf{p})] (|\mathbf{J}_2|^2 + |\mathbf{J}_3|^2) \\
&\quad + 2 \text{Re} [(\mathbf{J}_3^* - \mathbf{J}_2^*) \cdot \{ \mathbf{p}_0 (\mathbf{J}_2 \cdot \hat{\mathbf{k}}) (\mathbf{p} \cdot \hat{\mathbf{k}}) \\
&\quad - \mathbf{p} (\mathbf{J}_3 \cdot \hat{\mathbf{k}}) (\mathbf{p}_0 \cdot \hat{\mathbf{k}}) \}] \\
&\quad - (E_0 E + 1 + \mathbf{p}_0 \cdot \mathbf{p}) (\mathbf{J}_2 \cdot \hat{\mathbf{k}}) (\mathbf{J}_3^* \cdot \hat{\mathbf{k}}) \\
&\quad + (\mathbf{J}_2 \cdot \mathbf{p}_0) (\mathbf{J}_3^* \cdot \mathbf{p}) - (\mathbf{J}_2 \cdot \mathbf{p}) (\mathbf{J}_3^* \cdot \mathbf{p}_0) \\
&\quad + E_0 J_1^* \{ \mathbf{J}_3 \cdot \mathbf{p} - (\mathbf{J}_2 \cdot \hat{\mathbf{k}}) (\mathbf{p} \cdot \hat{\mathbf{k}}) \} \\
&\quad + E J_1^* \{ \mathbf{J}_2 \cdot \mathbf{p}_0 - (\mathbf{J}_3 \cdot \hat{\mathbf{k}}) (\mathbf{p}_0 \cdot \hat{\mathbf{k}}) \} \\
&\quad + (\mathbf{J}_2 \cdot \mathbf{J}_3^*) \{ \mathbf{p}_0 \cdot \mathbf{p} - (\hat{\mathbf{k}} \cdot \mathbf{p}_0) (\hat{\mathbf{k}} \cdot \mathbf{p}) \} \} \} \quad (8)
\end{aligned}$$

while the consistent third-order RDP term reads

$$\begin{aligned}
\frac{d^3\sigma_{\text{RDP},2}^Z}{dkd\Omega_k d\Omega_p} &= \alpha^2 Z^3 r_e^2 \frac{kp(\mathbf{q} \cdot \mathbf{k})}{p_0 q D_0 D} N \\
&\quad \times \left\{ \frac{2}{\pi} \text{Re} \left[\left(\{ E_0 E - 1 - (\hat{\mathbf{k}} \cdot \mathbf{p}_0) (\hat{\mathbf{k}} \cdot \mathbf{p}) \} J_1 \right. \right. \right. \\
&\quad \left. \left. + E_0 \{ \mathbf{J}_3 \cdot \mathbf{p} - (\mathbf{J}_2 \cdot \hat{\mathbf{k}}) (\mathbf{p} \cdot \hat{\mathbf{k}}) \} \right. \right. \\
&\quad \left. \left. + E \{ \mathbf{J}_2 \cdot \mathbf{p}_0 - (\mathbf{J}_3 \cdot \hat{\mathbf{k}}) (\mathbf{p}_0 \cdot \hat{\mathbf{k}}) \} \right) \right] e^{i\Phi} \right\}. \quad (9)
\end{aligned}$$

In Eqs. (8) and (9), $\mathbf{k} = k\hat{\mathbf{k}}$ and

$$N = \frac{4\pi^2 a_0 a}{(e^{2\pi a_0} - 1)(e^{2\pi a} - 1)},$$

where $a_0 = (E_0/p_0)\alpha Z_s$ and $a = (E/p)\alpha Z_s$, while

$$\begin{aligned}
D_0 &= 2(E_0 k - \mathbf{p}_0 \cdot \mathbf{k}) & D &= 2(Ek - \mathbf{p} \cdot \mathbf{k}) \\
\mu &= 2(E_0 E + p_0 p - 1) & \text{and } x &= 1 - \frac{D_0 D}{\mu q^2}.
\end{aligned}$$

The phase Φ in Eq. (9) is given by

$$\Phi = a_0 \ln \left(\frac{q^2}{D} \right) - a \ln \left(\frac{\mu}{D} \right),$$

and the coefficients J_1 , J_2 and J_3 are

$$\begin{aligned}
J_1 &= 2 \left(\frac{E}{D_0} - \frac{E_0}{D} \right) \frac{V + ia x W}{q^2} \\
&\quad + 2i \frac{(1-x)W}{D_0 D} \left[E_0 a \left(\frac{\mu}{D} - 1 \right) - E a_0 \left(\frac{\mu}{D_0} + 1 \right) \right] \\
J_2 &= \frac{V + ia x W}{D q^2} \mathbf{q} - \frac{ia(1-x)W}{D_0 D} \left[\left(\frac{\mu}{D} - 1 \right) \mathbf{q} - \frac{\mathbf{P}}{p_0} \right] \\
J_3 &= \frac{V + ia x W}{D q^2} \mathbf{q} - \frac{ia_0(1-x)W}{D_0 D} \left[\left(\frac{\mu}{D_0} + 1 \right) \mathbf{q} - \frac{\mathbf{P}}{p} \right].
\end{aligned}$$

As for $V = {}_2F_1(-ia_0, ia; 1; x)$ and $W = {}_2F_1(1 - ia_0, 1 + ia; 2; x)$, ${}_2F_1$ denotes the Gaussian hypergeometric function with argument $x \in [0, 1]$ [AS70], while

$$\mathbf{P} = p_0 \mathbf{p} + p \mathbf{p}_0.$$

Due to their high complexity, the expressions (8) and (9) can only be integrated over Ω_p numerically. The evaluation of two hypergeometric functions at each point renders the computation demanding; for computational efficiency, the latter are implemented in the form of series expansions, and the results have been benchmarked against an arbitrary-precision library [Joh17]. Details on the numerical implementation can be found in the source repository [GSPD25].

The use of FSM wave functions is valid as long as

$$\frac{(\alpha Z)^2}{r} \sin \left(\frac{\vartheta_{pr}}{2} \right) \ll 1, \quad (10)$$

where ϑ_{pr} is the angle between \mathbf{p} and \mathbf{r} , and $r = \|\mathbf{r}\|$, the electron–nucleus separation [HN04]. This condition is satisfied for low atomic numbers at all angles and energies, but its validity is restricted to small angles for higher Z . In practice this approximation is sufficient since photon emission is concentrated in the forward direction at higher electron energies. The implications of this condition are further discussed in Sec. IV.

III. SCREENED ELECTRON–ION BREMSSTRAHLUNG: THE MULTI-YUKAWA MODEL

To evaluate the screening correction term in Eq. (2), the screened DDCS is derived in the first Born approximation. In this section, the latter is constructed by introducing an atomic form factor based on the multi-Yukawa model and inserting it into the Bethe–Heitler TDCS. Integration over the electron scattering solid angle is then carried out analytically to yield the corresponding DDCS.

A. Atomic Form Factor

From the Thomas–Fermi–Kirillov (TFK) or Yukawa (Y) approximate atomic potential models [KTT75, AP93] the form factor for the ion Z_s , $F_{Z_s}(q)$, may be expressed in the simple form¹

$$F_{Z_s}(q) = \frac{1}{Z} \frac{N_s}{1 + (qa_{Z_s}/2)^n}, \quad (11)$$

¹ Note that the present definition of the form factor differs from Refs. [KTT75, SPMB+23] by an overall factor of $1/Z$. Here we adopt the convention commonly used in the bremsstrahlung literature.

where $n = 3/2$ and $n = 2$ for the TFK and Y potentials, respectively. Here $a_{Z_s} = 2\lambda_{Z_s}/\alpha$ is the effective screening length, with λ_{Z_s} the screening parameter of the underlying Yukawa or TFK potential. It depends on the atomic model and the ionization state. In the small- q limit, the form factor reduces to $F_{Z_s}(q) \simeq N_s/Z$, in agreement with charge conservation.

For an atomic potential represented as a sum of multiple Yukawa (MY) terms, the AFF (11) takes the form

$$F_{Z_s}(q) = \frac{N_s}{Z} \sum_i \frac{A_{s,i}}{1 + (qa_{Z_s,i}/2)^2},$$

where $\{A_{s,i}\}_i$ denote the weights corresponding to each exponential for the different ionization levels. For normalization, we impose $\sum_i A_{s,i} = 1$. This formulation provides an accurate description of screening effects, regardless of the ionization state or the atomic species. We refer to the work by Savoye-Peysson *et al.* for a detailed description of the MY model and its underlying assumptions [SPMB+23]. Integration over ϕ and θ of the outgoing electron yields the DDCS in photon energy and emission angle

$$\frac{d^2\sigma_{Z_s}^{\text{MY}}}{dkd\Omega_k} = \int_0^\pi \int_0^{2\pi} \frac{d^3\sigma_{Z_s}^{\text{MY}}}{dkd\Omega_k d\Omega_p} d\phi \sin\theta d\theta.$$

B. Screened Cross Section

For a standard Yukawa ($n = 2$) model, fully analytic expressions for the DDCS have been obtained [FU58, Hau08]. In contrast, for the approximate Thomas-Fermi-Kirillov atomic model ($n = 3/2$), the rational exponent prevents a closed-form expression, and a numerical integration is therefore required.

In this section, a fully analytic expression is derived for a multi-Yukawa (MY) model using the MY series,

$$\{A_{s,i}, a_{Z_s,i}\}_i,$$

determined via the generalized Salvat moment method for arbitrary ionization states [SMMP87, SPMB+23].

Combining Eq. (3) with the AFF Eq. (11),

$$\begin{aligned} \frac{d^3\sigma_{Z_s}^{\text{MY}}}{dkd\Omega_k d\Omega_p} &= \alpha \left(\frac{r_e}{2\pi}\right)^2 Z^2 \times \\ &\left(1 - (1 - qZ_s) \sum_i \frac{A_{s,i}}{1 + (qa_{Z_s,i}/2)^2}\right)^2 \frac{p}{kp_0 q^4} A^{\text{BH}}, \end{aligned} \quad (12)$$

where the term $qZ_s := Z_s/Z$, ranging between 0 and 1, characterizes the level of ionization, 0 being the neutral atom. Defining $b_{s,i} := 2/a_{Z_s,i}$, Eq. (12) may then be rewritten in the form

$$\frac{d^3\sigma_{Z_s}^{\text{MY}}}{dkd\Omega_k d\Omega_p} = \left(\sum_i A_{s,i} \frac{q^2 + qZ_s b_{s,i}^2}{q^2 + b_{s,i}^2}\right)^2 \frac{d^3\sigma_Z^{\text{BH}}}{dkd\Omega_k d\Omega_p}. \quad (13)$$

From now on, we omit the BH superscript on the Bethe-Heitler TDCS for the sake of readability. For a neutral atom, $qZ_0 = 0$, so

$$\frac{d^3\sigma_{Z_0}^{\text{MY}}}{dkd\Omega_k d\Omega_p} = q^4 \left(\sum_i \frac{A_{0,i}}{b_{0,i}^2 + q^2}\right)^2 \frac{d^3\sigma_Z}{dkd\Omega_k d\Omega_p},$$

a form already found in Ref. [Hau08].

For partially ionized atoms, the complexity is considerably higher because of the presence of the terms $\propto qZ_s A_{s,i} b_{s,i}^2$. Let us define

$$c_{s,i}^2 := qZ_s b_{s,i}^2,$$

which mixes ionization and screening, so the more symmetric form

$$\frac{d^3\sigma_{Z_s}^{\text{MY}}}{dkd\Omega_k d\Omega_p} = \left(\sum_i A_{s,i} \frac{c_{s,i}^2 + q^2}{b_{s,i}^2 + q^2}\right)^2 \frac{d^3\sigma_Z}{dkd\Omega_k d\Omega_p}$$

is obtained leveraging the positivity of qZ_s . For the usual Y potential with a single exponential, $i = 1$ and since $A_{s,1} = 1$ by definition,

$$\begin{aligned} \frac{d^3\sigma_{Z_s}^{\text{Y}}}{dkd\Omega_k d\Omega_p} &= \frac{d^3\sigma_Z}{dkd\Omega_k d\Omega_p} \{ \}, \\ \{ \} &= c_s^4 I_{2,0}(b_s, q) \\ &\quad + 2c_s^2 I_{2,1}(b_s, q) + I_{2,2}(b_s, q), \end{aligned} \quad (14)$$

where

$$I_{l,m}(b, q) = \frac{q^{2m}}{(b^2 + q^2)^l}.$$

When screening effects are neglected, $b_s = c_s = 0$, so only the last term in expression (14) remains. In this case, the Bethe-Heitler TDCS is correctly recovered since $I_{2,2}(0, q) = 1$. Conversely, for neutral atoms with screening ($c_{0,s} = 0, b_{0,s} \neq 0$) and

$$\frac{d^3\sigma_{Z_0}^{\text{Y}}}{dkd\Omega_k d\Omega_p} = I_{2,2}(b_0, q) \frac{d^3\sigma_Z}{dkd\Omega_k d\Omega_p},$$

which is similar to the expression found in [Hau08].

Having established the robustness of the construction through multiple checks, we now derive the doubly-differential cross section for the general MY case. When several exponentials are considered, the screening factor

$$\left(\sum_i A_{s,i} \frac{c_{s,i}^2 + q^2}{b_{s,i}^2 + q^2}\right)^2$$

is fully expanded by developing the four terms of the product. The TDCS for a MY potential then reads

$$\begin{aligned}
\frac{d^3 \sigma_{Z_s}^{\text{MY}}}{dk d\Omega_k d\Omega_p} &= \frac{d^3 \sigma_Z}{dk d\Omega_k d\Omega_p} \\
&\times \left\{ \sum_i A_{s,i}^2 [c_{s,i}^4 I_{2,0}(b_{s,i}, q) + 2c_{s,i}^2 I_{2,1}(b_{s,i}, q) + I_{2,2}(b_{s,i}, q)] \right. \\
&+ \sum_{i \neq i'} \frac{A_{s,i} A_{s,i'}}{(b_{s,i'}^2 - b_{s,i}^2)} [c_{s,i}^2 c_{s,i'}^2 (I_{1,0}(b_{s,i}, q) - I_{1,0}(b_{s,i'}, q)) \\
&+ (c_{s,i}^2 + c_{s,i'}^2) (I_{1,1}(b_{s,i}, q) - I_{1,1}(b_{s,i'}, q)) \\
&\left. + I_{1,2}(b_{s,i}, q) - I_{1,2}(b_{s,i'}, q)] \right\}. \tag{15}
\end{aligned}$$

The latter expression (15) must be integrated over the scattering directions Ω_p to obtain the screened, ionized doubly differential cross section. It is easily verified that upon setting $c_{s,i} = 0$, the neutral case from [Hau08] is recovered and that in the unscreened limit $b_{s,i}^2 \downarrow 0$, the Bethe–Heitler TDCS is retrieved. Let us define the double integrals $\mathcal{H}_{l,m}$ for $m \in \{0, 1, 2\}$ and $l \in \{1, 2\}$,

$$\mathcal{H}_{l,m}(b, q) := \int_0^\pi \int_0^{2\pi} \frac{d^3 \sigma_Z}{dk d\Omega_k d\Omega_p} I_{l,m}(b, q) d\phi \sin \theta d\theta,$$

$$= \int_0^\pi \int_0^{2\pi} \frac{d^3 \sigma_Z}{dk d\Omega_k d\Omega_p} \frac{q^{2m}}{(b^2 + q^2)^l} d\phi \sin \theta d\theta.$$

Note that in order to determine the screened DDCCS, only the integrals $\mathcal{H}_{1,m}(b)$ ought to be determined explicitly, since $\mathcal{H}_{2,m}(b) = -\partial \mathcal{H}_{1,m}(b) / \partial b^2$, as a consequence of the relation

$$\frac{\partial I_{1,m}(b)}{\partial b^2} = -\frac{q^{2m}}{(b^2 + q^2)^2} = -I_{2,m}(b).$$

Thus the DDCCS in presence of screening, with the MY model, becomes

$$\begin{aligned}
\frac{d^2 \sigma_{Z_s}^{\text{MY}}}{dk d\Omega_k} &= \sum_i A_{s,i}^2 [c_{s,i}^4 \mathcal{H}_{2,0}(b_{s,i}) + 2c_{s,i}^2 \mathcal{H}_{2,1}(b_{s,i}) + \mathcal{H}_{2,2}(b_{s,i})] \\
&+ \sum_{i \neq i'} \frac{A_{s,i} A_{s,i'}}{(b_{s,i'}^2 - b_{s,i}^2)} [c_{s,i}^2 c_{s,i'}^2 (\mathcal{H}_{1,0}(b_{s,i}) - \mathcal{H}_{1,0}(b_{s,i'})) \\
&+ (c_{s,i}^2 + c_{s,i'}^2) (\mathcal{H}_{1,1}(b_{s,i}) - \mathcal{H}_{1,1}(b_{s,i'})) \\
&+ (\mathcal{H}_{1,2}(b_{s,i}) - \mathcal{H}_{1,2}(b_{s,i'}))]. \tag{16}
\end{aligned}$$

Note that for the Y model ($i = 1$), the cross-terms vanish and expression (16) reduces to the much simpler

$$\begin{aligned}
\frac{d^2 \sigma_{Z_s}^{\text{Y}}}{dk d\Omega_k} &= c_s^4 \mathcal{H}_{2,0}(b_s) \\
&+ 2c_s^2 \mathcal{H}_{2,1}(b_s) + \mathcal{H}_{2,2}(b_s).
\end{aligned}$$

The $\mathcal{H}_{l,m}$ integrals can be expressed in terms of the analytical results by Fronsdal and Überall [FU58], for which we use the notation from [Hau08], I_1 and I_2 :

$$\begin{aligned}
\mathcal{H}_{1,0}(b) &= \frac{I_2(b^2) - I_2(0) + b^2}{b^4} \\
\mathcal{H}_{1,1}(b) &= \frac{I_2(0) - I_2(b^2)}{b^2}
\end{aligned}$$

$$\begin{aligned}
\mathcal{H}_{1,2}(b) &= I_2(b) \\
\mathcal{H}_{2,0}(b) &= 2 \frac{I_2(b^2) - I_2(0) + b^2}{b^6} + \frac{I_1(b^2) - 1}{b^4} \\
\mathcal{H}_{2,1}(b) &= \frac{I_2(0) - I_2(b^2)}{b^4} - \frac{I_1(b^2)}{b^2} \\
\mathcal{H}_{2,2}(b) &= I_1(b^2).
\end{aligned}$$

The I_1 and I_2 integrals read

$$\begin{aligned}
I_1(b) &= \frac{\alpha Z^2 r_0^2}{2\pi k p_0} \left\{ 16 p (4E_0^2 + b^2) \frac{\|\mathbf{p}_0 \times \mathbf{k}\|^2}{k^2 W^4} \right. \\
&\left. - \frac{2p}{W^2} \left[4E_0^2 + 2E_0 E - E \frac{D_1}{k} + b^2 \left(1 - 2E \frac{k}{D_1} \right) \right] \right\}
\end{aligned}$$

$$\begin{aligned}
& + \frac{2p}{W^2} \frac{D_1^2 + 2(E_0E - 1)D_1 + b^2(D_1 - 2Ek)}{(D_1 + b^2)^2 + 4p^2b^2} \\
& \times \left[\frac{1}{D_1} (16E_0E - 4E_0^2b^2 - b^4) - \frac{4E_0^2 + b^2}{k^2W^2} \right. \\
& \left. \times \{D_1^2 + 2(E_0E - 1)D_1 + b^2(D_1 - 2Ek)\} \right] \\
& - \frac{2k^2p}{(D_1 + b^2)^2 + 4p^2b^2} \left[\frac{4}{D_1^2} (4E_0^2 + (1 - D_1)b^2) \right. \\
& \left. + \frac{D_1^2 + 2(E_0E - 1)D_1 + b^2(D_1 - 2Ek)}{D_1 \|\mathbf{p}_0 - \mathbf{k}\|^2} \right] \\
& - \frac{4k}{D_1} \ln(E + p) + \frac{L_1}{W} \left[2k + \frac{4k}{D_1} (E_0^2 + p^2 + b^2) \right. \\
& \left. + \frac{2}{D_1W^2} (E_0D_1 - 2k + b^2k) \right. \\
& \left. \times \left(8E_0E - \frac{D_1^2}{2} - b^2(2E_0^2 + 2p^2 + D_1) - b^4 \right) \right. \\
& \left. + \frac{2(2E_0^2 + b^2)(D_1 - 2Ek) + D_1^2 + 2(E_0E - 1)D_1}{k W^2} \right. \\
& \left. - \frac{3}{k W^4} (4E_0^2 + b^2) \left(E_0 \frac{D_1}{k} - 2 + b^2 \right) \right. \\
& \left. (D_1^2 + 2(E_0E - 1)D_1 + b^2(D_1 - 2Ek)) \right] \\
& + \frac{k^2 L_2}{D_1 \|\mathbf{p}_0 - \mathbf{k}\|} \left[\frac{2}{D_1} - 2 + \frac{D_1 - 2Ek}{2 \|\mathbf{p}_0 - \mathbf{k}\|^2} \right] \Bigg\},
\end{aligned}$$

and

$$\begin{aligned}
I_2(b) = & - \frac{\alpha Z^2 r_0^2}{2\pi k p_0} \left\{ \frac{2p(4E_0^2 + b^2)}{W^2} \left(E_0 \frac{D_1}{k} - 2 + b^2 \right) \right. \\
& + \frac{L_1}{W} \left[k(D_1 + 2b^2) \right. \\
& \left. + \frac{2k}{D_1} (b^4 + 2b^2(E_0^2 + p^2) - 8E_0E) \right] \\
& + \frac{4E_1^2 + b^2}{kW^2} \left(D_1^2 + 2(E_0E - 1)D_1 \right. \\
& \left. + b^2(D_1 - 2Ek) \right) \\
& + \frac{k^2 L_2}{D_1 \|\mathbf{p}_0 - \mathbf{k}\|} \left[\frac{2}{D_1} (4E^2 + b^2(1 - D_1)) \right. \\
& \left. + \frac{D_1^2 + 2(E_0E - 1)D_1 + b^2(D_1 - 2Ek)}{2 \|\mathbf{p}_0 - \mathbf{k}\|^2} \right] \\
& \left. - \frac{4k}{D_1} b^2 \ln(E + p) \right\}.
\end{aligned}$$

The quantities involved in I_1 and I_2 are given by

$$\begin{aligned}
D_1 & = 2k (E_0 - p_0 \cos \theta_1) \\
W & = \left[\left(p_0 \frac{D_1}{k} \right)^2 + 2b^2 \left(E_0 \frac{D_1}{k} - 2 \right) + b^4 \right]^{1/2} \\
L_1 & = \ln \frac{(E_0E - 1) D_1/k + E b^2 + p W}{(E_0E - 1) D_1/k + E b^2 - p W} \\
L_2 & = \ln \frac{(\|\mathbf{p}_0 - \mathbf{k}\| + p)^2 + b^2}{(\|\mathbf{p}_0 - \mathbf{k}\| - p)^2 + b^2}.
\end{aligned}$$

Equation (16) is a *fully analytical* expression of the screened doubly differential cross section (DDCS) for *arbitrary ionized states* described by a multi-Yukawa (MY) potential. That result, together with Eq. (5) and the numerical integration of Eq. (7), enables the evaluation of the total DDCS Eq. (2).

IV. CROSS SECTION RESULTS

The equations (5), (7), and (16) have been implemented in a MATLAB program [GSPD25]. While Eqs. (5) and (16) can be evaluated directly from their analytical forms, the RDP contribution is evaluated by numerically integrating the TDCS in Eq. (7) over the scattering angles (θ, ϕ) using an adaptive grid method, achieving a relative accuracy better than 10^{-6} [GSPD25].

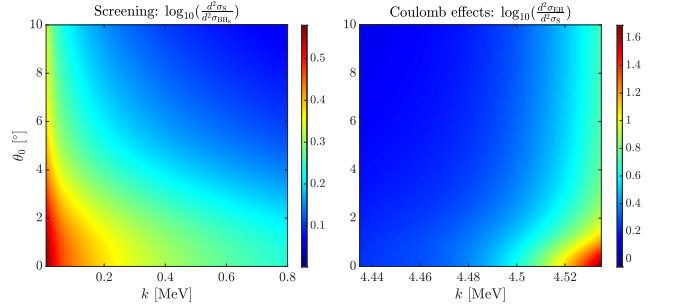


Figure 1. Left: Region of the parameter space where the screening is prominent, namely soft-photons and forward emissions, for an incoming electron of energy $E_0 = 4.54$ MeV on a gold target. Right: Region of the parameter space where Coulomb corrections are required, i.e. hard photons and forward emissions. In the ratios, $d^2\sigma$ stands for $d^2\sigma/dk d\Omega_k$.

Figure 1 provides physical motivation for the separation of screening and Coulomb contributions embodied in the Olsen–Maximon–Wergeland (OMW) formulation, Eq. (2). The left panel shows the logarithm of the ratio between the unscreened (Sauter) reference and the corresponding screened Bethe–Heitler (multi-Yukawa) DDCS, as a function of the emitted photon energy and emission angle, for an incident electron energy of $E_0 = 4.54$ MeV. This representation highlights the importance of screening effects, which are most pronounced in the soft-

photon, forward-emission domain. The right panel displays the logarithm of the ratio of the leading-order RDP (Elwert–Haug) cross section to Sauter’s Coulomb-field result, illustrating the onset of Coulomb (nuclear) corrections toward forward angles and higher photon energies. Because the next-to-leading-order RDP expression is not reliable in the high-frequency (tip) region, the leading-order result is used in the ratio shown.²

Figure 1 is intended to illustrate the physical motivation for treating the screening correction additively in Eq. (2); a detailed assessment of the OMW additivity rule can be found in Ref. [JAM19].

To assess the consistency of the analytical DDCS for partially ionized species, results from the closed-form expression (16) are compared with those obtained by direct numerical integration of Eq. (13) for all ionization states of a given atom. Fig. 2 shows an excellent agreement for several ionization degrees of aluminum ($Z = 13$), where two Yukawa exponentials have been used for the description of the potential. As expected, in the screening-dominant (large wavelength) region, the emission increases with the ionization state, i.e. with the effective ion charge Z_s . The fully stripped limit is Sauter’s expression Eq. (5) for a pure Coulomb field. The neutral case Z_0 corresponds by definition to the expression found by Haug [Hau08], except that in the present model the number of exponentials is Z -dependent and not fixed to three, allowing a better fitting of the atomic potential.

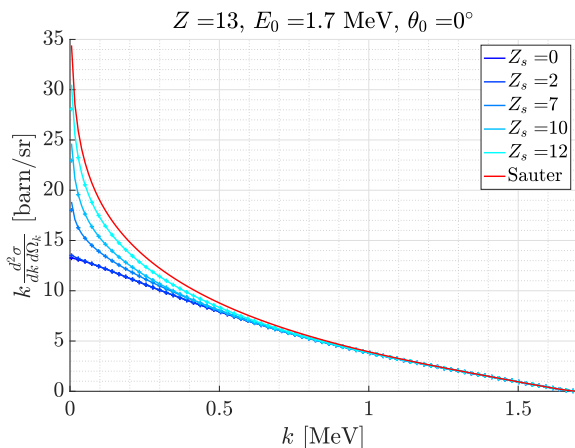


Figure 2. Comparison of the DDCS obtained from the closed form Eq. (16) (solid lines) and from a numerical integration of Eq. (13) (markers), for several ionized states of aluminum, and two Yukawa exponentials.

² The next-to-leading-order RDP theory was derived under the assumption that both the incident and scattered electron energies are large, and therefore loses accuracy in the high-frequency (tip) region.

A. Multi-Yukawa and Ionized Cross Sections

This section analyzes the influence of the multi-Yukawa potential representation on the bremsstrahlung emission cross sections of partially ionized species, highlighting the model’s internal consistency and physical trends.

We begin by examining how the atomic form factor (AFF) is influenced by the number of exponentials, N_Y , used in the multi-Yukawa model. The top panel of Fig. 3 shows the AFF as a function of the nuclear recoil momentum for a neutral copper atom, calculated with several values of N_Y and compared with the “exact” form factor obtained from density-functional theory (DFT) [WJB⁺22, SPMB⁺23] using the GAUSSIAN code [FTS⁺16]. The bottom panel of Fig. 3 illustrates the corresponding impact on the doubly differential cross section (DDCS). The incident-electron energy is set to 1.7 MeV, and two small emission angles, 0° and 5° , are considered, since screening effects are most pronounced in the forward direction. As expected, the DDCS increases slightly with N_Y , because the screening factor for $N_Y = 1$

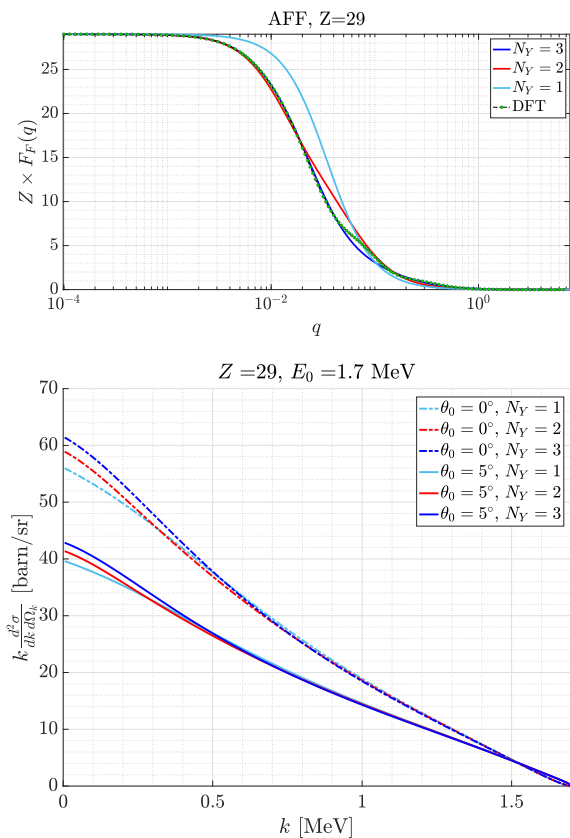


Figure 3. Top: Atomic form factor for a neutral copper atom ($Z = 29$) as a function of the recoil momentum, calculated with one, two, and three Yukawa exponentials, and compared with the reference form factor obtained from DFT. Bottom: Neutral doubly photon energy, for one, two, and three Yukawa exponentials and for two emission angles.

is larger than for $N_Y = 2, 3$ at low values of q .

The DDCS is calculated for various ionized states of gold ($Z = 79$) and is shown in Fig. 4. Although the cross section is monotonically increasing with the ion charge Z_s for low values of k , a minimum is found at non-neutral states for higher photon energies.

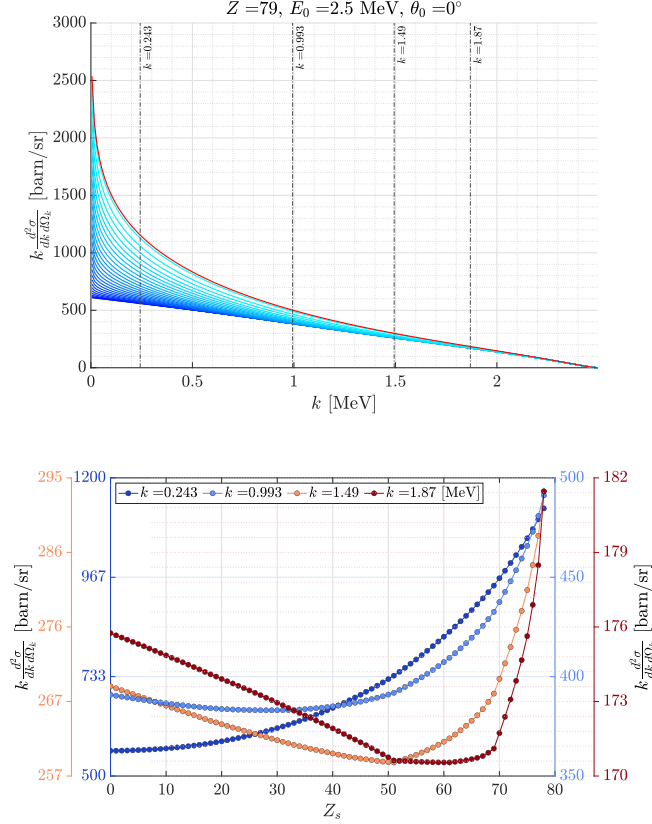


Figure 4. Top: Ionized doubly differential cross section (DDCS) for gold. Every third ionization level is shown; the red line represents Sauter's model. Vertical lines indicate the photon energies for which the DDCS is plotted as a function of ionization level in the bottom inset. Bottom: DDCS for gold at the four photon energies indicated above.

The non-monotonic behavior of the doubly differential cross section with increasing ionization state at higher photon energies k originates from the atomic form factor, which reflects the effective nuclear charge experienced during the interaction. At higher photon energies, the form factor does not vary monotonically with Z_s , as illustrated in Fig. 5, where F_{Z_s} is plotted as a function of the recoil momentum $q(k)$ for several ionization states.

Since the atomic form factor is the Fourier transform of the spatial electronic density n_s ,

$$F_{Z_s}(q) = \frac{1}{Z} \int_{\mathbb{R}^3} n_s(\mathbf{r}) e^{i\mathbf{q}\cdot\mathbf{r}} d^3r$$

$$= 1 - \sum_i A_i \frac{q^2 + qZ_s b_i^2}{q^2 + b_i^2},$$

where \mathbf{r} is in units of the reduced Compton wavelength and n_s is rescaled accordingly so as to preserve its normalization, the relative behavior of the form factors for different ionization states is strongly influenced by the corresponding radial electron densities around the nucleus. When these densities cross, the form factors can exhibit similar non-monotonic behavior.

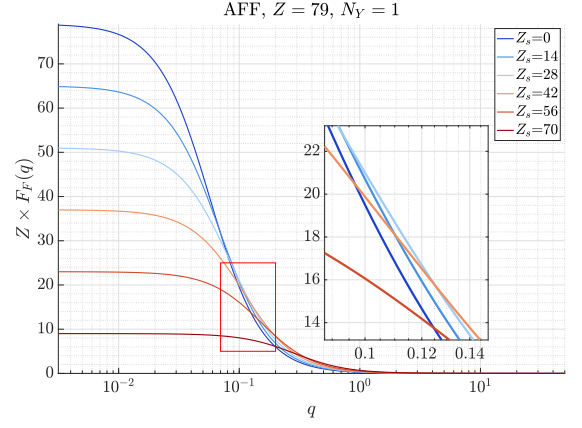


Figure 5. Atomic form factor for several ionization states of gold, and one Yukawa exponential. The form factor exhibits some crossings of the ionized curves, as emphasized by a zoom in the red rectangle.

For each ionization state of gold shown in Fig. 5, the corresponding radial bound-electron density is displayed in the top inset of Fig. 6. Because the crossings between the density profiles are not clearly visible, the largest intersection radius between each reference profile and higher ionized states has been determined. The resulting characteristic intersection radii are presented in the bottom panel of Fig. 6.

The intersection radius between two radial bound-electron density profiles, $n_s(r)$ and $n_{s'}(r)$, provides a convenient way to visualize how ionization modifies the spatial extent of the electronic cloud. If the bound-electron distribution contracted strictly monotonically with increasing ionization, no radial crossings would occur. Each more-ionized state would be confined to a smaller radius. Conversely, a radial crossing between n_s and $n_{s'}$ indicates that upon removing electrons, the residual bound charge has redistributed onto a larger characteristic shell at a certain radius, so that the screening length is increased rather than decreased. Among the possible intersections, the outermost crossing is the most physically relevant, as it occurs in the outer region of the atom where the residual bound-electron density dominates and thus determines the long-range screening behavior (low q -domain). The presence of such crossings therefore indicates that the contraction of the electronic cloud with ionization is not perfectly monotonic: the residual electrons undergo redistribution which in turn leads to the non-monotonic behavior of the atomic form factor $F_{Z_s}(q)$ with ionization, as observed in Fig. 5.

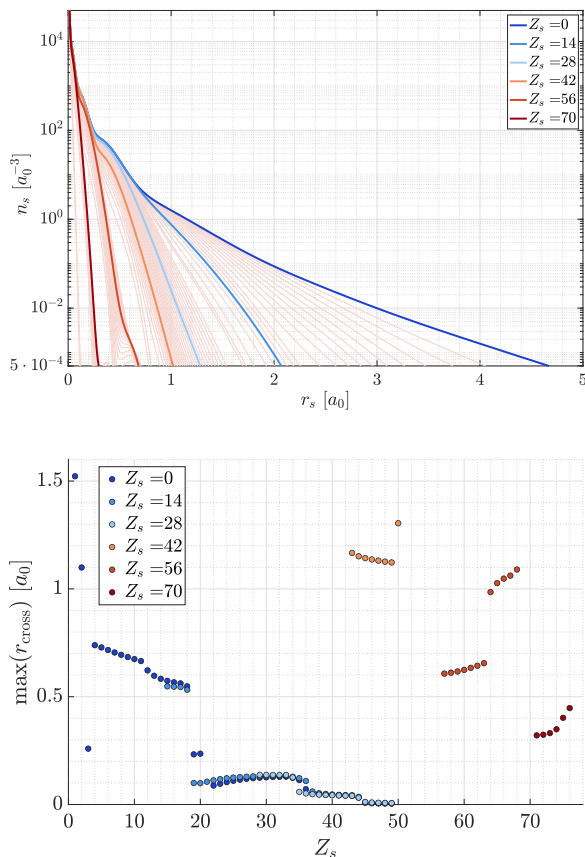


Figure 6. Top: Bound-electron density profiles for all ionization states of gold, calculated using DFT with the GAUSSIAN code [FTS⁺16]. The upper blue curve corresponds to the neutral atom and the ionization degree increases from right to left. Bottom: Largest intersection radius between each reference density (highlighted in the legend) and all higher ionization states for a gold atom.

The existence of non-monotonic behaviors in the screened cross section illustrated in Fig. 4, is systematically observed across different incident electron energies, emission angles, and atomic numbers. Since the formulation is constrained by fully relativistic *ab initio* density functional theory calculations, the resulting electronic densities can be regarded as essentially exact. The observed effect therefore reflects intrinsic atomic-physics behavior rather than a model-dependent artifact. Whereas this feature does not appear in approximate models such as the Tseng–Pratt–Avdonina–Lamoureux formulation, it is found in several alternative descriptions that incorporate comparable physical ingredients, including the Thomas–Fermi [Tho27, Fer28], Thomas–Fermi–Kirillov [KTT75], and Tseng–Pratt–Botto [BMP78, WJB⁺22] models. A detailed comparison among these screening formalisms lies however beyond the scope of the present work.

B. Comparison with Data for the Doubly Differential Cross Section

The screening model developed in Section III and analyzed in Section IV A is combined with the exact Coulomb bremsstrahlung correction at the doubly differential level through Eq. (2). This formulation enables direct comparison with experimental measurements in the neutral state for arbitrary atomic species, electron and photon energies, and emission angles.

A substantial amount of experimental data is available in the literature for thin-target bremsstrahlung measurements of the doubly differential cross section (DDCS), covering incident electron energies from a few keV up to about 10 MeV [Mot55, SK56, MP58, KM59, RD67, EH69, RE72, LKPT76]. In the present study, three representative elements—Al, Sn, and Au—are selected to span low to high atomic numbers and to sample different combinations of incident-electron energy and emission angle. The experimental data of Starfelt and Koch [SK56] and of Rester and Dance [RD67] are employed for direct comparison with the model, in accordance with other recent analyses [MM16, MM17, JAM19].³

In Figs. 7, 8, 9, the solid red lines represent the Sauter formula, Eq. (5); the dashed green curves correspond to the multi-Yukawa Born approximation, Eq. (16); and the dashed blue curves show the integrated RDP result, Eq. (7). The total cross section obtained from Eq. (2) is plotted as a dashed black line. Measurement uncertainties include statistical errors (error bars), which affect both the spectral shape and the absolute magnitude of the cross sections, and systematic errors, which influence only the absolute magnitude [SK56, RD67]. The contours represent the combined statistical and systematic uncertainties.

For low atomic numbers, the agreement between the model and experiments is excellent over the entire range of photon energies and emission angles, as shown in the two uppermost plots of Fig. 7. For higher atomic numbers, the model agrees well with experimental measurements of emission in the forward $\leq 10^\circ$ direction. However, as illustrated in the lower right-hand panel of Fig. 7 shows that both the Born-approximation cross sections (Sauter and screened Bethe–Heitler) and the FSM-based RDP cross section fail to reproduce the experimental data accurately for high atomic number and large emission angle. This tendency was also noted for tin, although with smaller magnitude. The explanation is a combined breakdown of the Born approximation, as the condition

$$\frac{\alpha Z_s}{\beta_0}, \frac{\alpha Z_s}{\beta} \ll 1 \quad (17)$$

³ Some results by Rester and Dance were previously obtained by Motz [Mot55], but they differ significantly from both the later measurements of Rester and Dance and from theoretical predictions. For this reason, they are not considered in the present work.

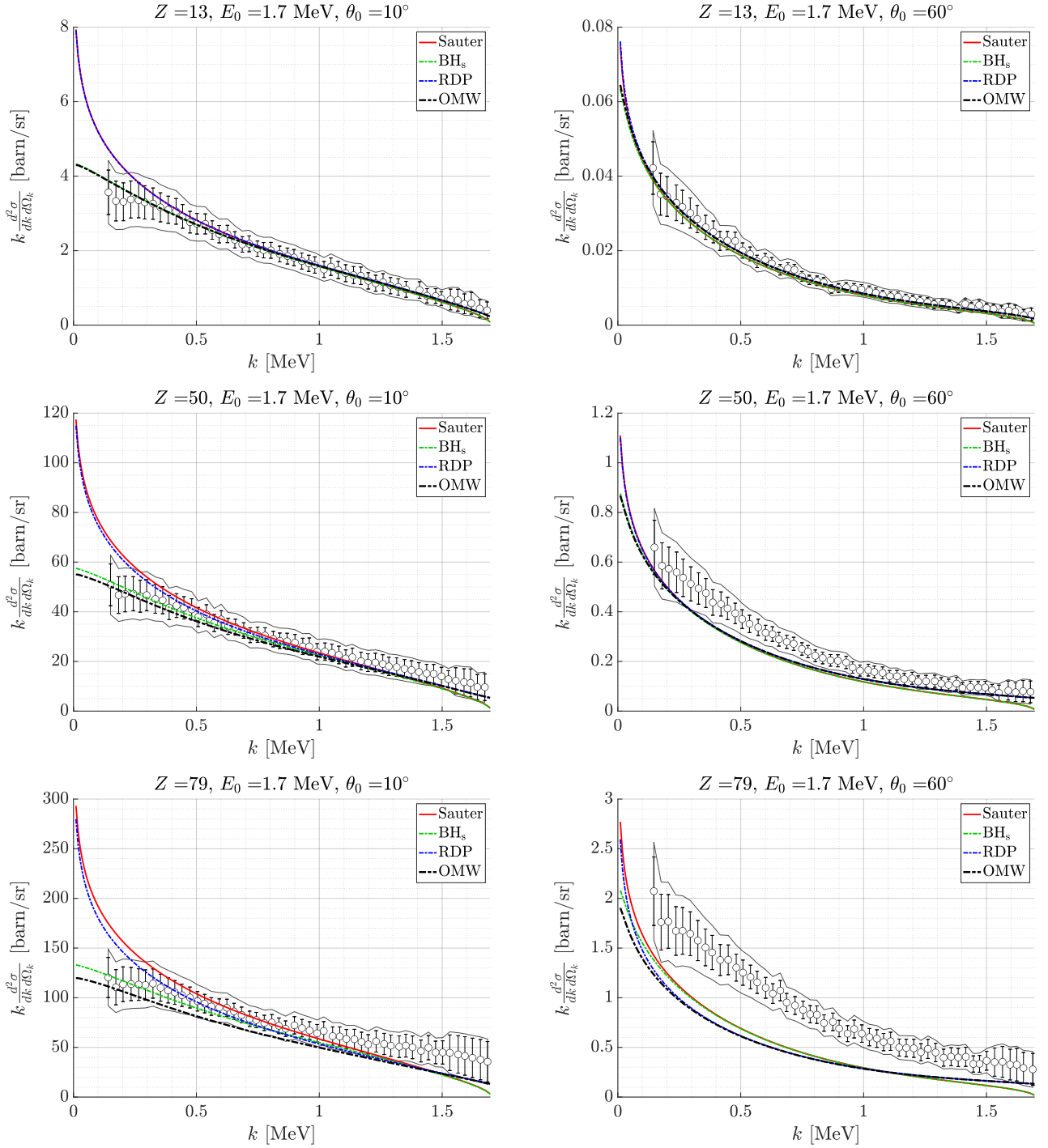


Figure 7. Comparison of the theoretical model components against the experimental results by Rester and Dance [RD67], for aluminum, tin and gold. The error bars represent statistical uncertainties, while the contours indicate the sum of the statistical and systematic errors. The incoming electron has an energy of 1.7 MeV.

is no longer satisfied, and of the FSM wave-function validity. The breakdown of the FSM condition is likely the dominant cause, given that Eq. (17) contains no angular dependence, and the lower-left panel ($Z = 79, \theta_0 = 10^\circ$) does not reveal any obvious failure of the Born-based cross sections (Sauter and screened Bethe–Heitler).

At larger angles, where screening effects are weaker, the Sauter and Bethe–Heitler results are expected to approach each other, since the screening correction within the Born approximation becomes small. In this regime, the dominant contribution should therefore arise from the RDP cross section, which lies significantly below the ex-

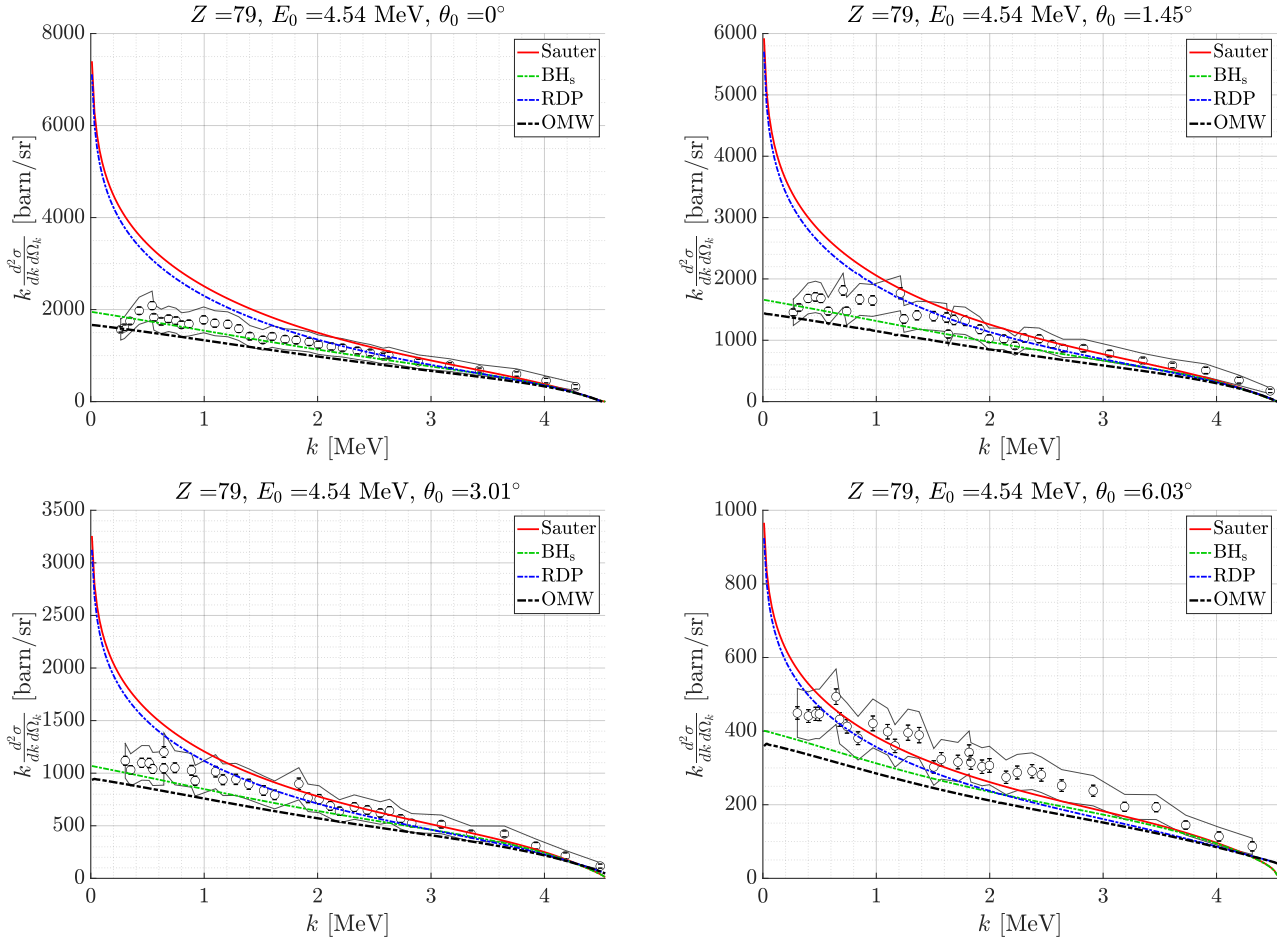


Figure 8. Comparison of the theoretical model components against the experimental results by Starfelt and Koch [SK56], for gold at several low angles where the screening is important. The error bars represent statistical uncertainties, while the contours indicate the sum of the statistical and systematic errors. The incoming electron has an energy of 4.54 MeV.

perimental values for $\theta_0 = 60^\circ$, consistent with the breakdown of the FSM approximation in the high- q region.⁴ It is however important to note that the corresponding cross sections are two orders of magnitude lower than those obtained for emissions at 10° .

The onset of this behavior also appears at smaller emission angles for higher incident electron energies, as shown by comparison with data in Figs. 8 and 9. The validity of the FSM condition (10) becomes increasingly restricted at higher incident energies, since the momentum transferred to the nucleus, q , rises for a given emission angle,

probing smaller distances from the nucleus according to $r \sim 1/q$ [HN04]. As the relevant interaction radius decreases, the local deflection ϑ_{pr} of the electron in the Coulomb field grows, and the FSM approximation can fail even for comparatively small observable angles. This trend is evident in Fig. 8 for 4.54 MeV electrons incident on gold ($Z = 79$), where a noticeable discrepancy between the model and the experimental measurements already appears at $\theta_0 \simeq 6^\circ$. At such angles, however, the corresponding emission intensity is an order of magnitude lower than in the purely forward direction ($\theta_0 = 0^\circ$). It is important to note that in the near-forward direction ($\theta_0 \sim 0^\circ$), the RDP cross section decreases sharply in the high-frequency limit, in a manner similar to the Born results (see the two upper panels of Fig. 8). Although this behavior is mitigated as the emission angle increases, the RDP cross section cannot be expected to be accurate in the tip region, since the next-to-leading-order correction relies on the assumption that the scattered electron remains highly relativistic. By contrast, the leading-order (EH) cross section does not exhibit such a decrease in the

⁴ Note that Furry–Sommerfeld–Maue condition (10) involves the local angle ϑ_{pr} between the electron momentum and its position vector in the Coulomb field, rather than the measured photon emission angle θ_0 . Although these two quantities are distinct, they are correlated through the recoil momentum $\mathbf{q} = \mathbf{p}_0 - \mathbf{p} - \mathbf{k}$ as larger q corresponds to smaller effective electron–nucleus separations and therefore to stronger local deflections [HN04]. The FSM approximation is expected to deteriorate in regions of large q , which typically occur for large emission angles.

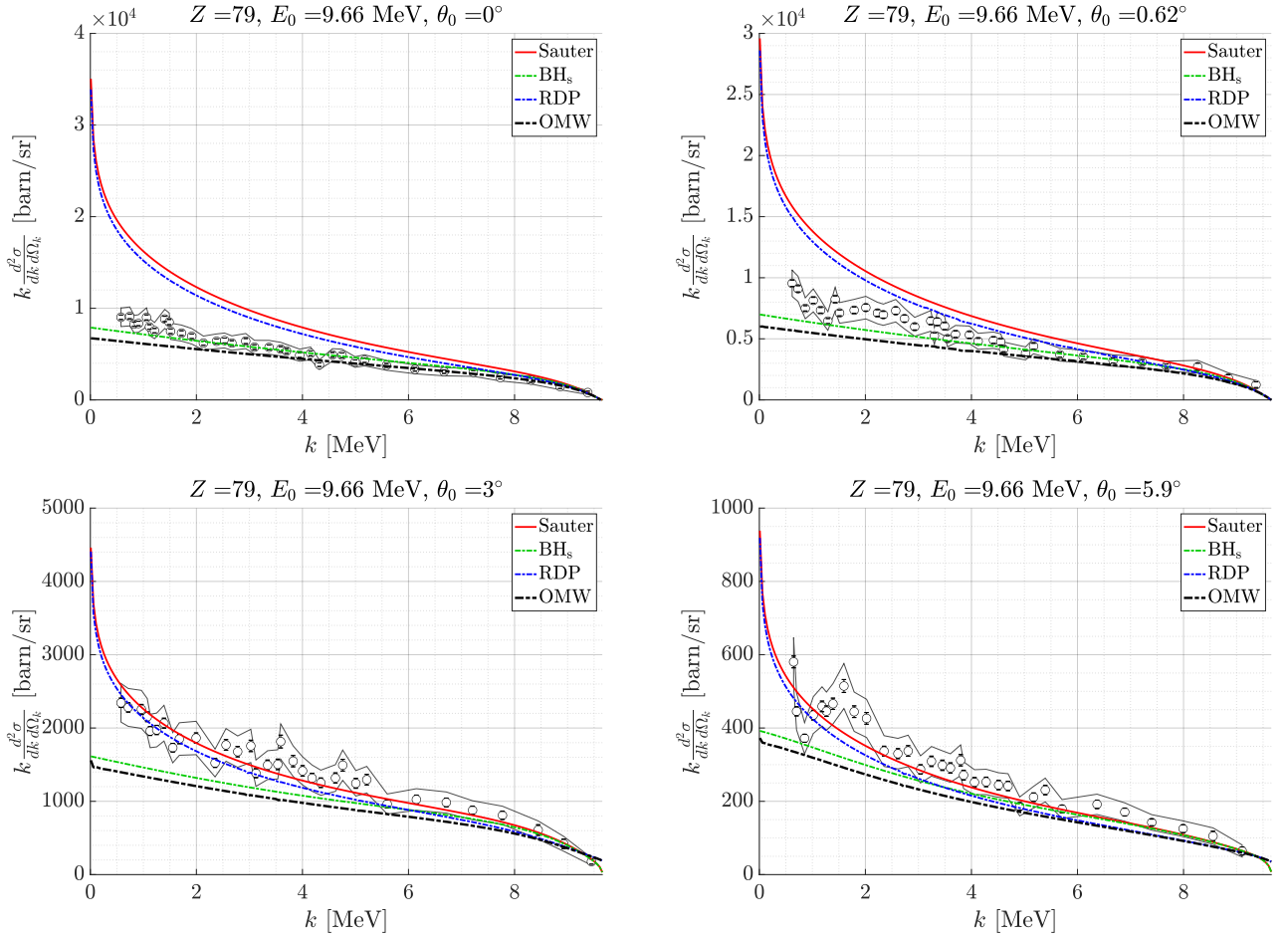


Figure 9. Comparison of the theoretical model components against the experimental results by Starfelt and Koch [SK56], for gold at several low angles where the screening is important. The error bars represent statistical uncertainties, while the contours indicate the sum of the statistical and systematic errors. The incoming electron has an energy of 9.66 MeV.

tip region, although it is not shown here. As the emission angle increases, all theoretical components (RDP, Sauter, and BH_s) shift downward relative to the experimental data, such that their combination, Eq. (2), lies systematically below the measurements, even though these angles remain smaller than in Fig. 7.

A similar trend is observed when comparing with the highest available thin-target bremsstrahlung cross sections, measured at an incident electron energy of 9.66 MeV. As shown in Fig. 9, the theoretical components exhibit a consistent downward displacement relative to the experimental points.

At these higher energies, an additional source of uncertainty arises from the photomultiplier response function used by Starfelt and Koch, which was obtained through Monte Carlo simulations performed by other authors [SK56]. Nevertheless, the systematic downward shift of all theoretical components strongly indicates that the principal cause of the discrepancy is the breakdown of the FSM approximation in the high- q regime, where the local perturbative expansion ceases to hold.

Roche, Ducos, and Proriot originally indicated that their formulation remains applicable up to electron energies of approximately 50 MeV [RDP72]. In the present work, this framework is employed in its consistently ordered form (see Eq. (9)). Figure 10 shows the components of the model in Eq. (2) for an incident electron energy of 30 MeV on a gold target. The various contributions behave consistently and exhibit no qualitative discrepancies relative to the trends observed at lower energies. The choice of 30 MeV corresponds to approximately three times the highest incident energy for which experimental data are currently available. These results suggest that the present formulation can reasonably be applied at such energies, provided the system remains in a regime where the breakdown of the FSM approximation is limited. When the FSM approximation is no longer adequate, an exact treatment of the Coulomb field using Dirac wave functions provides a natural alternative, assuming that screening corrections can still be incorporated additively within the OMW framework.

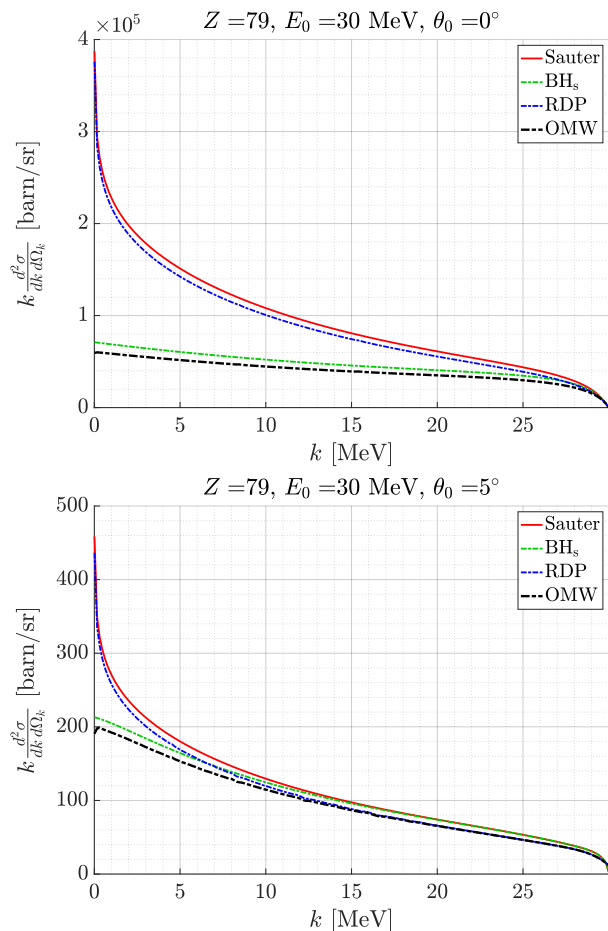


Figure 10. Top: Theoretical model components for a 30 MeV electron incident on gold, with emission at $\theta_0 = 0^\circ$. Bottom: Identical, for $\theta_0 = 5^\circ$.

V. CONCLUSION AND OUTLOOKS

In this paper, the general formalism describing the calculation of bremsstrahlung differential cross sections was reviewed, addressing the main challenges still faced by existing theoretical models. The commonly adopted expression for the doubly differential cross section (DDCS) is based on the cross section in a pure Coulomb field, calculated within the Furry–Sommerfeld–Maue (FSM) picture and corrected for screening effects in the Born approximation. The novelty of the present work lies in a new formulation of the screening correction such that (i) the model accounts for screening in partially ionized states, and (ii) the correction is expressed in fully analytic form, allowing instantaneous evaluation and efficient exploration of large parameter spaces. In addition, the Coulomb-field contribution entering this formulation was evaluated using the corrected next-to-leading-order Roche–Ducos–Proriol (RDP) expression.

The partially screened DDCS was obtained by extending the Bethe–Heitler cross section through the inclusion of an atomic form factor representing par-

tially ionized states, described by a multi-Yukawa potential [SPMB⁺23]. Building on existing results for neutral screened bremsstrahlung, an analytical expression was derived for arbitrary ionization levels.

The model was applied to a range of atomic numbers, emission angles, and incident electron energies, while varying internal parameters such as the number of Yukawa exponentials used to represent the screened potential. The results show that the emission intensity does not increase monotonically with ionization: for certain photon energies, a minimum appears at higher ionization levels. This behavior arises from the non-monotonic dependence of the atomic form factors on ionization, which reflects oscillations in the radial bound-electron densities as the ionization state changes.

The performance of the screened model of Eq. (2) in the neutral case was evaluated by comparison with experimental measurements across a range of atomic numbers, emission angles, and incident electron energies. Excellent agreement was obtained for forward emission angles and incident energies up to about 5 MeV, from low- to high- Z elements. At larger emission angles, the model systematically underestimates the measured spectra, consistent with previous observations [MM16, MM17, JAM19]. This discrepancy is attributed to the breakdown of the FSM approximation at larger deflection angles and becomes apparent at smaller angles as the energy increases. However, this limitation is not critical, since cross sections in these regions are several orders of magnitude smaller than in forward emission. In practical situations, angular integration and the finite spatial and momentum spread of the electron beam further increase the contribution of forward emission.

Addressing the identified limitations may require moving beyond the present set of approximations and solving the Dirac equation for exact electron wave functions in the screened potential of ionized atoms. Such an extension would be computationally demanding but represents a natural direction for future work. Additionally, new and extended experimental data would be highly valuable for further benchmarking and refinement of the models.

DATA AVAILABILITY STATEMENT

The data that support the findings of this article are openly available [GSPD25].

ACKNOWLEDGMENTS

The authors are indebted to A. Mangiarotti for providing some of the tabulated experimental data, and thankful to A. Mangiarotti and K. Barbey for valuable discussions.

AUTHOR CONTRIBUTIONS

S. Guinchard: Conceptualization (equal); Formal analysis (equal); Methodology (lead); Software (equal); Writing – original draft (lead); Writing – review & editing (lead). **Y. Savoye-Peysson:** Conceptualization (equal); Formal analysis (equal); Software (equal); Writing – review & editing (equal). **J. Decker:** Formal analysis (equal); Software (equal); Writing – review & editing (equal).

REFERENCES

- [AP93] N. B. Avdonina and R. H. Pratt. Bremsstrahlung spectrum from ions in a model potential approximation. *J. Quant. Spectrosc. Radiat. Transfer*, 50(4):349–358, 1993.
- [AS70] M. Abramowitz and I. A. Stegun. *Handbook of mathematical functions*. Dover Publication, New York, USA, 9th edition, 1970.
- [BH34] H. Bethe and W. Heitler. On the stopping of fast particles and on the creation of positive electrons. In The Royal Society Publishing (London), editor, *Proceedings of the Royal Society of London*, volume 146, pages 83–112, 1934.
- [BM54] H. Bethe and L. C. Maximon. Theory of bremsstrahlung and pair production. i. differential cross section. *Phys. Rev.*, 93(4):768–784, 1954.
- [BMP78] David J. Botto, James McEnnan, and R. H. Pratt. Analytic description of photoeffect from atomic ions. *Phys. Rev. A*, 18:580–586, Aug 1978.
- [CRB20] Jens Chluba, Andrea Ravenni, and Boris Bolliet. Improved calculations of electron–ion bremsstrahlung Gaunt factors for astrophysical applications. *Mon. Not. Roy. Astron. Soc.*, 492(1):177–194, 2020.
- [EH69] G. Elwert and E. Haug. Calculation of bremsstrahlung cross sections with sommerfeld-maue eigenfunctions. *Phys. Rev.*, 183(1):90–105, 1969.
- [Elw39] Gerhard Elwert. Verschärfte berechnung von intensität und polarisation im kontinuierlichen röntgenspektrum. *Annalen der Physik*, 426(2):178–208, 1939.
- [Fer28] E. Fermi. Eine statistische methode zur bestimmung einiger eigenschaften des atoms und ihre anwendung auf die theorie des periodischen systems der elemente. *Zeitschrift für Physik*, 48(1):73–79, 1928.
- [Fer50] Enrico Fermi. *Nuclear Physics: A Course Given by Enrico Fermi at the University of Chicago*. University of Chicago Press, Chicago, 1950.
- [FGJB19] C. Froese Fischer, G. Gaigalas, P. Jonsson, and Bieron. Grasp2018-a fortran 95 version of the general relativistic atomic structure package. *Computer Physics Communications*, 237:184–187, 2019.
- [FTS⁺16] M. J. Frisch, G. W. Trucks, H. B. Schlegel, G. E. Scuseria, M. A. Robb, J. R. Cheeseman, G. Scalmani, V. Barone, G. A. Petersson, H. Nakatsuji, X. Li, M. Caricato, A. Marenich, J. Bloino, B. G. Janesko, R. Gomperts, B. Mennucci, H. P. Hratchian, J. V. Ortiz, A. F. Izmaylov, J. L. Sonnenberg, D. Williams-Young, F. Ding, F. Lipparini, F. Egidi, J. Goings, B. Peng, A. Petrone, T. Henderson, D. Ranasinghe, V. G. Zakrzewski, J. Gao, N. Rega, G. Zheng, W. Liang, M. Hada, M. Ehara, K. Toyota, R. Fukuda, J. Hasegawa, M. Ishida, T. Nakajima, Y. Honda, O. Kitao, H. Nakai, T. Vreven, K. Throssell, J. A. Montgomery, Jr., J. E. Peralta, F. Ogliaro, M. Bearpark, J. J. Heyd, E. Brothers, K. N. Kudin, V. N. Staroverov, T. Keith, R. Kobayashi, J. Normand, K. Raghavachari, A. Rendell, J. C. Burant, S. S. Iyengar, J. Tomasi, M. Cossi, J. M. Millam, M. Klene, C. Adamo, R. Cammi, J. W. Ochterski, R. L. Martin, K. Morokuma, O. Farkas, J. B. Foresman, and D. J. Fox. Gaussian 09, revision e.01. Technical report, Gaussian, Inc., Wallingford CT, 2016.
- [FU58] C. Fronsdal and H. Überall. Polarization of bremsstrahlung from polarized electrons. *Phys. Rev.*, 111:580–586, Jul 1958.
- [Fur34] W. H. Furry. Approximate wave functions for high energy electrons in coulomb fields. *Phys. Rev.*, 46:391–396, Sep 1934.
- [Fur51] W. H. Furry. On bound states and scattering in positron theory. *Phys. Rev.*, 81:115–124, Jan 1951.
- [GSPD25] Salomon Guinchard, Yves Savoye-Peysson, and Joan Decker. Thin-target bremsstrahlung cross sections. 10.5281/zenodo.17507210, November 2025. Software.
- [Hau08] E. Haug. Bremsstrahlung cross-section with screening and coulomb corrections at high energies. *Radiation Physics and Chemistry*, 207:207–214, 2008.
- [HN04] E. Haug and W. Nakel. *The Elementary Process of Bremsstrahlung*. World Scientific lecture notes in physics. World Scientific, 2004.
- [HVB⁺75] J. H. Hubbell, Wm. J. Veigele, E. A. Briggs, R. T. Brown, D. T. Cromer, and R. J. Howerton. Atomic form factors, incoherent scattering functions, and photon scattering cross sections. *Journal of Physical and Chemical Reference Data*, 4(3):471–538, 07 1975.
- [JA21] D. H. Jakubassa-Amundsen. Theoretical approaches for hard electron bremsstrahlung and their scaling properties in the ultrarelativistic regime. *Phys. Rev. A*, 104:052802, Nov 2021.
- [JAM19] D. H. Jakubassa-Amundsen and A. Mangiarotti. Accuracy of analytical theories for relativistic bremsstrahlung. *Phys. Rev. A*, 100:032703, Sep 2019.
- [Joh17] Fredrik Johansson. Arb: Efficient arbitrary-precision midpoint-radius interval arithmetic. *IEEE Transactions on Computers*, 66(8):1281–1292, 2017.
- [JR55] Josef M Jauch and Fritz Rohrlich. *The theory of photons and electrons: the relativistic quantum field theory of charged particles with spin one-half*. Springer Science & Business Media, 1955.
- [KM59] H. W. Koch and J. W. Motz. Bremsstrahlung cross-section formulas and related data. *Rev. Mod. Phys.*, 31:920–955, Oct 1959.
- [KMTY88] R. Kawakami, K. Mima, H. Totsuji, and Y. Yokoyama. Bremsstrahlung from hot, dense, partially ionized plasmas. *Phys. Rev. A*, 38:3618–3627, Oct 1988.
- [KTT75] V. D. Kirillov, B.A. Trubnikov, and S.A. Trushin. Role of impurities in anomalous plasma resistance. *Fizika Plazmy*, 1:218 – 237, Mar - Apr 1975.
- [LKPT76] C. M. Lee, Lynn Kissel, R. H. Pratt, and H. K. Tseng. Electron bremsstrahlung spectrum, 1-500 keV. *Phys. Rev. A*, 13:1714–1727, May 1976.
- [LP53a] L. D. Landau and I. Pomeranchuk. Electron cascade process at very high-energies. *Dokl. Akad. Nauk Ser. Fiz.*, 92:735–738, 1953.
- [LP53b] L. D. Landau and I. Pomeranchuk. Limits of applicability of the theory of bremsstrahlung electrons and pair

- production at high-energies. *Dokl. Akad. Nauk Ser. Fiz.*, 92:535–536, 1953.
- [MdAG87] Leonard C. Maximon, Arlette de Miniac, Thierry Aniel, and Eric Ganz. Tagged photons: An analysis of the bremsstrahlung cross section. *Physics Reports*, 147(4):189–252, 1987.
- [Mig56] A. B. Migdal. Bremsstrahlung and pair production in condensed media at high energies. *Phys. Rev.*, 103:1811–1820, Sep 1956.
- [MJA17] A. Mangiarotti and D. H. Jakubassa-Amundsen. Higher-order theories for relativistic electron-atom bremsstrahlung in comparison with experiment. *Phys. Rev. A*, 96:042701, Oct 2017.
- [MM16] A. Mangiarotti and M. N. Martins. Higher-order corrections to electron-nucleus bremsstrahlung cross sections above a few MeV. *Phys. Rev. A*, 94:022708, Aug 2016.
- [MM17] A. Mangiarotti and M.N. Martins. A review of electron–nucleus bremsstrahlung cross sections between 1 and 10MeV. *Radiation Physics and Chemistry*, 141:312–338, 2017.
- [Mol47] Gert Moliere. Theorie der streuung schneller geladener teilchen i. einzelstreuung am abgeschirmten coulomb-feld. *Zeitschrift für Naturforschung A*, 2:133–145, 1947.
- [Mot55] J. W. Motz. Bremsstrahlung differential cross-section measurements for 0.5- and 1.0-mev electrons. *Phys. Rev.*, 100:1560–1571, Dec 1955.
- [MP58] J. W. Motz and R. C. Placius. Bremsstrahlung cross-section measurements for 50-keV electrons. *Phys. Rev.*, 109:235–242, Jan 1958.
- [OMW57] Haakon Olsen, L. C. Maximon, and Harald Wergeland. Theory of high-energy bremsstrahlung and pair production in a screened field. *Phys. Rev.*, 106(1):27–46, 1957.
- [PD08] Y. Peysson and J. Decker. Fast electron bremsstrahlung in axisymmetric magnetic configuration. *Phys. Plasmas*, 15(9):092509, 2008.
- [PT75] R. H. Pratt and H. K. Tseng. Tip region of the bremsstrahlung spectrum from incident electrons of kinetic energy 50 keV–1.84 MeV. *Phys. Rev. A*, 11(6):1797–1803, 1975.
- [PTL⁺77] R.H. Pratt, H.K. Tseng, C.M. Lee, Lynn Kissel, Crawford MacCallum, and Merle Riley. Bremsstrahlung energy spectra from electrons of kinetic energy $1 \text{ keV} \leq t_1 \leq 2000 \text{ keV}$ incident on neutral atoms $2 \leq Z \leq 92$. *Atomic Data and Nuclear Data Tables*, 20(2):175–209, 1977.
- [Rac34] Giulio Racah. Sopra l’irradiazione nell’urto di particelle veloci. *Il Nuovo Cimento (1924-1942)*, 11(7):461–476, 1934.
- [RD67] D. H. Rester and W. E. Dance. Bremsstrahlung cross-section measurements at incident electron energies of 1.0, 1.7, and 2.5 MeV. *Phys. Rev.*, 161:85–93, Sep 1967.
- [RDP72] G. Roche, C. Ducos, and J. Proriol. Bremsstrahlung cross-section formula including a high-order coulomb correction. *Phys. Rev. A*, 5(6):2403–2408, 1972.
- [RE72] D. H. Rester and N. Edmonson. Bremsstrahlung cross-section measurements at an incident electron energy of 0.2 MeV on Al, Cu, and Au. *Phys. Rev. A*, 6:1405–1409, Oct 1972.
- [Sau34] Fritz Sauter. Über die bremsstrahlung schneller elektronen. *Annalen der Physik*, 412(4):404–412, 1934.
- [Sch68] Leonard I. Schiff. *Quantum Mechanics*. McGraw-Hill, New York, 3rd edition, 1968.
- [SK56] N. Starfelt and H. W. Koch. Differential cross-section measurements of thin-target bremsstrahlung produced by 2.7- to 9.7-MeV electrons. *Phys. Rev.*, 102:1598–1612, Jun 1956.
- [SM35] A. Sommerfeld and A. W. Maue. Verfahren zur näherungsweise anpassung einer lösung der schrödinger-an die diracgleichung. *Annalen der Physik*, 414(7):629–642, 1935.
- [SMMP87] F. Salvat, J. D. Martinez, R. Mayol, and J. Parelada. Analytical dirac-hartree-fock-slater screening function for atoms ($Z = 1-92$). *Phys. Rev. A*, 36(2):467–474, 1987.
- [SPMB⁺23] Y. Savoye-Peysson, D. Mazon, J. Bielecki, D. Dworak, K. Krol, A. Jardin, M. Scholz, J. Walkowiak, and J. Decker. A unified description of the atomic physics for electron fokker-planck calculations. *Nucl. Fusion*, 63:126041, 2023.
- [Sum04] H. P. Summers. The adas user manual, version 2.6. Technical report, ADAS, 2004.
- [Tho27] L. H. Thomas. The calculation of atomic fields. *Mathematical Proceedings of the Cambridge Philosophical Society*, 23(5):542–548, 1927.
- [TP71] H. K. Tseng and R. H. Pratt. Exact screened calculations of atomic-field bremsstrahlung. *Phys. Rev. A*, 3:100–115, Jan 1971.
- [WJB⁺22] J. Walkowiak, A. Jardin, J. Bielecki, Y. Peysson, D. Mazon, D. Dworak, K. Król, and M. Scholz. Approximate atomic models for fast computation of the fokker–planck equation in fusion plasmas with high-Z impurities and suprathermal electrons. *Physics of Plasmas*, 29(2):022501, 02 2022.
- [YS10] Vladimir A. Yerokhin and Andrey Surzhykov. Electron-atom bremsstrahlung: Double-differential cross section and polarization correlations. *Phys. Rev. A*, 82:062702, Dec 2010.